Magnetic Resonance Study of MnO/ZnO Nanopowders

N. Guskos[a,b], G. Zolnierkiewicz[b], J. Typek[b,*], D. Sibera[c], U. Narkiewicz[c] and W. Łojkowski[d]

[a]Solid State Section, Department of Physics, University of Athens, Panepistimiopolis, 15 784, Greece

[b]Institute of Physics, West Pomeranian University of Technology, al. Piastów 48, 70-311 Szczecin, Poland

[c]Institute of Chemical and Environmental Engineering, West Pomeranian University of Technology al. Piastów 17, 70-310 Szczecin, Poland

[d]Institute of High Pressure Physics, Polish Academy of Sciences, Sokołowska 29/37, 01-142 Warsaw, Poland

(Received May 18, 2011)

Fine particles $n(\mathrm{MnO})/(1-n)\mathrm{ZnO}$ ($n = 0.05$ to 0.95) were prepared by wet chemistry method. According to X-ray diffraction analysis the obtained samples with $n = 0.95$, 0.90, 0.80, 0.70, 0.60 contained Mn_3O_4 and $ZnMn_2O_4$ phases, while samples with $n = 0.05$, 0.10, 0.20, 0.30, 0.40 and 0.50 contained $ZnMnO_3$ and ZnO phases. The mean crystalline size of $ZnMnO_3$ varied from 8 to 13 nm. The magnetic resonance investigations have been carried out at room temperature. Slightly asymmetric, broad and intense magnetic resonance line is recorded for all samples. The magnetic resonance spectra parameters showed marked differences depending on the composition index n. This could be explained by the variation of the magnetic susceptibility and a much slower evolution of spin relaxation, associated with the interaction of crystal field and superexchange interactions. Taking into account the values of magnetic resonance parameters, the investigated samples could be divided into two groups: these with the composition index $n < 0.50$ and those with $n > 0.50$. A detailed discussion of the magnetic properties of different phases in the $n(\mathrm{MnO})/(1-n)\mathrm{ZnO}$ system is presented.

PACS: 75.50.Tt, 76.30.Fc, 76.50.+g

1. Introduction

In the recent years a lot of attention is devoted to theoretical and experimental study of a group of materials called diluted magnetic semiconductors (DMS) [1]. A serious obstacle in finding practical applications for these materials is the stabilization of their interesting physical properties at room temperature (thus their Curie temperature should be higher than 300 K). Despite initial promising results obtained for the compound ZnO:Mn [2], it is not clear at the present moment whether this material could be useful in technological applications. The main unsolved problem in DMS materials is the origin and nature of their magnetism [3]. In several cases magnetism was the result of segregation of metal agglomerates while in other cases the presence of transitional metals with different valences coupled by the double exchange mechanism was crucial [4, 5]. Recent research points to a very important role played by the defects [6]. For example, in ZnO:Mn in form of nanoparticles or thin films the ferromagnetism has appeared at room temperature only when the particle were capped by molecules introducing defects of the p-type [6]. Quite the opposite effect was observed for thin films of ZnO:Co in which ferromagnetism at high temperature was observed only in the presence of n-type defects [7]. It was found that the magnetic properties of ZnO:Co and ZnO:Mn strongly depended on thermal annealing in different atmospheres [8]. Moreover, doping of ZnO thin films with non-magnetic ions from the $3d$ group (e.g. titanium or vanadium) can cause emergence of ferromagnetic properties [9]. All these results indicate on a critical role of electronic structure of a semiconductor (modified by the presence of magnetic ions) in appearance of ferromagnetic properties.

Another interesting property of ZnO nanoparticles, particularly in UV-A range, is the blocking of UV radiation. This allows employment of these nanoparticles in cosmetic industry as well as in fabrication of paints and fibers [10]. High catalytic activity of these nanoparticles is a disadvantage in oxidation and photochemical reactions. However, it is possible to reduce it by modification of the surfaces of nanoparticles [11]. Applications of ZnO nanoparticles seem particularly promising in the area of optoelectronic devices. They find employment as blue light sources, in the form of nanotubes as radiation emitters of UV, also in biology and medicine as fluores-

* corresponding author; e-mail: typjan@zut.edu.pl

cence markers [12]. Recently, the electron paramagnetic resonance/ferromagnetic resonance (EPR/FMR) investigation of n(FeO)/$(1-n)$ZnO samples with $n < 0.70$ showed that the magnetic resonance line originates from the isolated iron(III) ions in zinc ferrite (EPR line) while for higher concentrations of iron oxide it could be attributed to the γ-Fe_2O_3 magnetic nanoparticles (FMR line) [13, 14].

The aim of this report is to study the EPR/FMR spectra of a series of n(MnO)/$(1-n)$ZnO ($n = 0.05$ to 0.95) nanopowders prepared by wet chemistry method. A wide compositional range of the used two metal oxides would allow to obtain a more complete picture of magnetic properties of the n(MnO)/$(1-n)$ZnO system.

2. Experimental

The mixture of manganium and zinc hydroxides was obtained by addition of ammonia solution to 20% solution of proper amount of $Zn(NO_3)_2{\cdot}6H_2O$ and $Mn(NO_3)_2{\cdot}4H_2O$ in water. The obtained hydroxides were filtered, dried and calcined at 300 °C for 1 h. A series of samples containing n(MnO)/$(1-n)$ZnO ($n = 0.05$ to 0.95) was obtained.

The phase composition of samples was determined using XRD (Co K_α radiation, X'Pert Philips). The mean crystallite size of these phases was determined using Scherrer's formula. The morphology of samples was investigated using scanning electron microscopy (LEO 1530).

The specific surface area of the nanopowders was determined by the Brunauer–Emmett–Teller (BET) method (nitrogen adsorption) using the equipment Gemini 2360 of Micromeritics. The helium pycnometer AccuPyc 1330 of Micromeritics was applied to determine the density of powders.

The measurements of magnetic resonance spectra were performed on conventional X-band ($\nu = 9.4$ GHz) EPR Bruker E 500 spectrometer with 100 kHz magnetic field modulation. Samples containing around 20 mg of powder were placed in 4 mm diameter quartz tubes. The measurements were carried out at room temperature.

3. Results and discussion

Figure 1 presents the XRD patterns of ZnO doped with MnO demonstrating the presence of spinel, manganium oxide and zinc oxide phases in the system. In samples n(MnO)/$(1-n)$ZnO ($n = 0.05$ to 0.50) (Fig. 1A) two phases: ZnO (number of the corresponding card is 89-0510 ICDD) and $ZnMnO_3$ (number of the corresponding card is 19-1461 ICDD) are observed. With increasing MnO concentration the content of ZnO phase decreases and the peak attributed to this phase disappears in sample containing 60 wt% of MnO (40 wt% of ZnO) (Fig. 1B). The peak of ZnO disappears, because all zinc is now bonded in the spinel phase (Fig. 2). In samples containing 60 wt% MnO and more, the phases of $ZnMn_2O_4$ (number of the corresponding card is 77-0470 ICDD) and Mn_3O_4 (number of the corresponding card is 80-0382 ICDD) are found. XRD method was applied to determine a mean crystallite size in prepared samples, using the Scherrer formula. It was calculated that the mean crystallite size of $ZnMnO_3$ varied from 8 to 13 nm, depending on the content of MnO (Fig. 3) as determined on the basis of the detailed analysis of the peak at the angle $2\Theta = 43$.

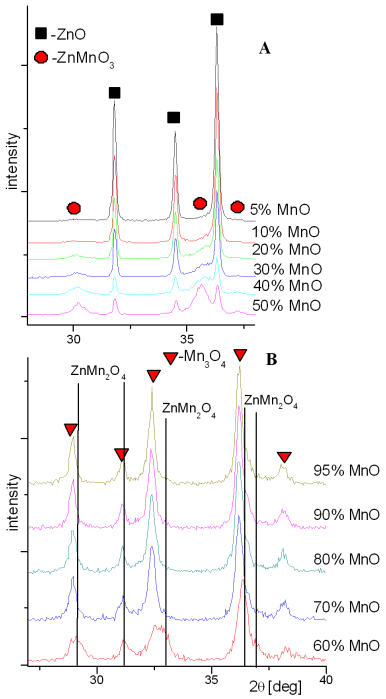

Fig. 1. The XRD patterns of ZnO doped MnO. (A) Peaks attributed to ZnO are marked as ■, peaks attributed to $ZnMnO_3$ are marked as •. (B) Peaks attributed to Mn_3O_4 are marked as ▼, peaks attributed to $ZnMn_2O_4$ are marked as vertical line.

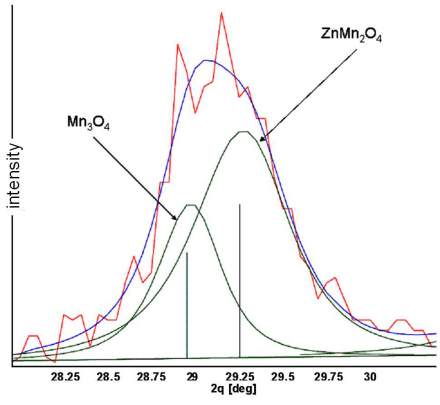

Fig. 2. Deconvolution of a single XRD line for sample n(MnO)/$(1-n)$ZnO with $n = 0.60$.

TABLE

The values of magnetic resonance spectra parameters (H_r — resonance field, g_{eff} — effective g-factor, ΔH_{pp} — peak-to-peak linewidth, I_n — integrated intensity) for different values of composition index n in $n(MnO)/(1-n)ZnO$ nanopowders.

Composition index n in $n(MnO)/(1-n)ZnO$ formula	H_r [G]	g_{eff}-factor	Linewidth ΔH_{pp} [G]	Integrated intensity ratio $I_n/I_{0.05}$
0.05	3362(3)	2.000(2)	741(1)	1
0.10	2020(3)	3.329(2)	481(1)	4557
0.20	3350(3)	2.007(2)	2480(2)	4034
0.30	3340(2)	2.011(2)	2600(2)	6038
0.40	3360(2)	2.001(2)	2700(2)	10669
0.50	3610(3)	1.863(2)	3500(3)	13225
0.60	3500(3)	1.921(2)	2200(2)	11200
0.70	3530(3)	1.905(2)	2350(2)	15201
0.80	3570(3)	1.883(2)	2350(2)	11700
	2670(3)	2.518(2)	106(1)	660
0.90	3560(3)	1.889(2)	2330(2)	14300
0.95	3560(3)	1.889(2)	2410(2)	15483

Figure 4 presents the results of specific surface area and density measurements. With the increase of ZnO content a drop of the specific surface area and an increase of density is registered. This is also illustrated by SEM images showing the morphology of specific samples (Fig. 5). The powders containing more manganese oxide are less agglomerated than samples with a lower content of MnO. Additionally, the agglomerates should be more stable, because the specific surface area drops from 14 m^2/g to 4 m^2/g.

Figure 6a–d presents the magnetic resonance spectra of a series of $n(MnO)/(1-n)ZnO$ samples containing from 5 to 95 wt% of MnO. The magnetic resonance spectra are dominated by a slightly asymmetric, intense, and broad line. The resonance lines of manganese ions are basically centered at $g_{eff} \approx 1.86$–2.02 with peak-to-peak linewidths ΔH_{pp} in the range of 480–3500 G. In Table the values of magnetic resonance spectra parameters (H_r — resonance field, g_{eff} — effective g-factor, ΔH_{pp} — peak-to-peak linewidth, I_n — integrated intensity) for different values of the composition index n in $n(MnO)/(1-n)ZnO$ nanopowders are given. The intensity of the observed spectra strongly depends on the concentration of magnetic ions.

Two spectral features are apparent in Fig. 6: a very broad and intense line and a six-line structure around $g \approx 2$. The broad line is typical for exchange coupled Mn ions, frequently observed in other Mn doped nanocrystals, while the six-line spectrum is usually attributed to Mn^{2+} incorporated in the nanocrystals. Closer inspection of Fig. 6b reveals an additional set of six-line structure. It could be attributed to Mn^{2+} ions in strongly distorted environment, e.g. on the surface of ZnO nanoparticles.

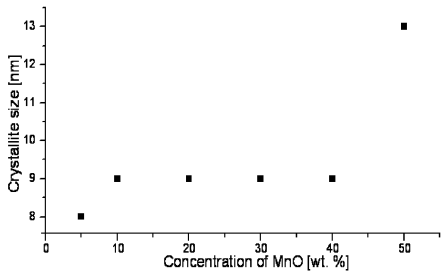

Fig. 3. The dependence of the mean crystallite size of $ZnMnO_3$ on the MnO phase concentration.

To make presentation of the obtained spectra more transparent, two-dimensional (g-factor, linewidth) representation of the magnetic resonance parameters of the investigated samples is presented in Fig. 7. The integrated intensity, which is calculated as the product of observed line amplitude and the square of linewidth, is proportional to magnetic susceptibility of the investigated spin system. In Fig. 8 comparison of the EPR relative integrated intensities (in logarithmic scale) of various $n(MnO)/(1-n)ZnO$ samples is shown. The integrated intensity of sample $n = 0.05$ was taken as a reference point.

For samples with high concentration of Mn(II) ions placed in an organic matrix the following values of g-factor and linewidth were observed: $g_{eff} = 2.0135(5)$ and $\Delta H_{pp} = 325(5)$ G [13]. Broadening of the EPR line is usually observed in anisotropic antiferromagnets due to the slowing down of spin fluctuations as the critical temperature is approached from above [14, 15]. Larger changes of linewidth and intensity than for the present samples were registered for the system $n(Fe_2O_3)/(1-n)ZnO$ [16]. Very small concentration of the EPR

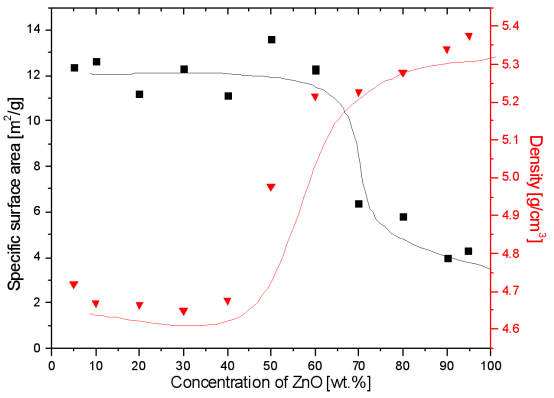

Fig. 4. The dependence of specific surface area (filled squares) and density (filled triangles) on the ZnO phase concentration.

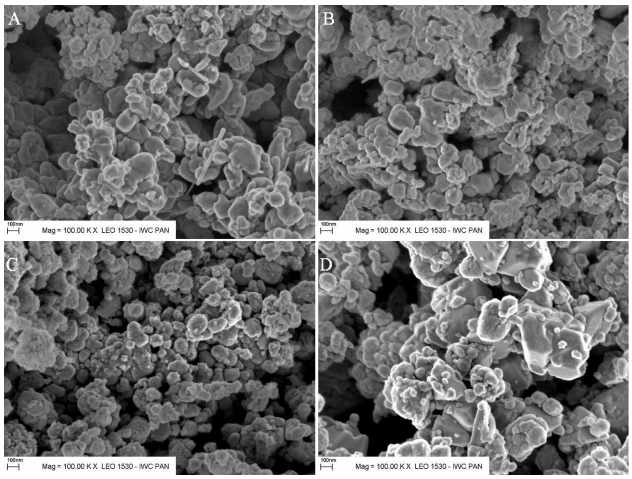

Fig. 5. SEM images of $n(\mathrm{MnO})/(1-n)\mathrm{ZnO}$ nanopowders: (A) $n = 0.95$, (B) $n = 0.80$, (C) $n = 0.50$, (D) $n = 0.20$.

spectra of isolated Mn(II) ions is recorded for samples with small contents of the manganese oxides, while maximum concentration was registered for sample with 30% of MnO. The resonance line for sample with 10% MnO shows a marked anomaly — it is shifted drastically in the direction of small magnetic field. Additionally, the presence of a spurious phase attributed to isolated Mn(II) ions is observed (Fig. 6d). It is suggested that an intense magnetic agglomeration process was in action and in effect the FMR spectrum was recorded. The $ZnMnO_3$ compound could be in ferromagnetic phase above room temperature [1, 17–19]. Low concentration of magnetic nanoparticle agglomerates could shift essentially the resonance line in the direction of small magnetic fields [20]. For this sample only a small concentration of $ZnMnO_3$ phase is observed which could be detected by XRD method (Fig. 1). An additional resonance line is observed for sample with 80% concentration of MnO (Fig. 6 and Table) which is shifted strongly in the direction of smaller

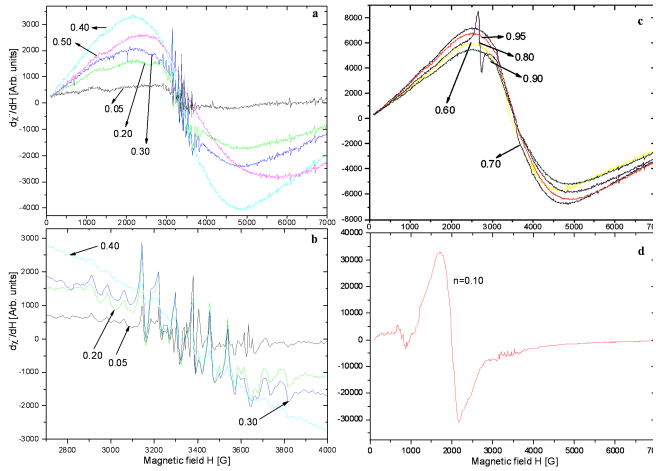

Fig. 6. The EPR/FMR spectra of $n(\mathrm{MnO})/(1-n)\mathrm{ZnO}$ ($n = 0.05$ to 0.95) nanopowders registered at room temperature: for $n = 0.05$, 0.20, 0.30, 0.40, 0.50 in a wide range of magnetic fields (a); for the same samples as in (a) but in a narrow range of magnetic fields around $g \approx 2.0$ (b); for $n = 0.60$, 0.70, 0.80, 0.90, 0.95 (c); for $n = 0.10$ (d).

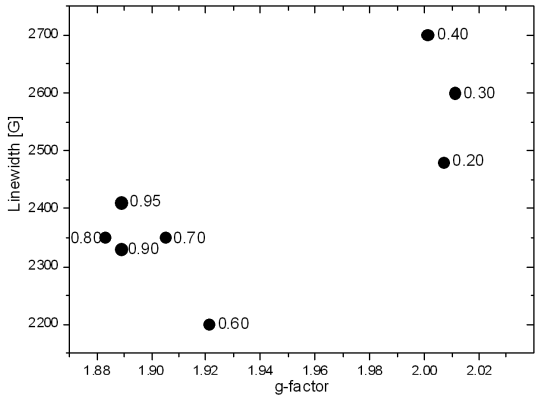

Fig. 7. Two-dimensional plot of g-factors and linewidths for $n(\mathrm{MnO})/(1-n)\mathrm{ZnO}$ nanopowders. The numbers by the experimental points are the values of the composition index n in $n(\mathrm{MnO})/(1-n)\mathrm{ZnO}$ formula.

magnetic fields. It could be assumed that the magnetic agglomeration process could be responsible for this shift.

As it is seen in Fig. 7, from the point of view of magnetic resonance parameters, the investigated samples could be divided into two groups: these with the composition index $n < 0.5$ and those with $n > 0.5$. In samples with $n < 0.5$ the magnetic response comes from the magnetic $ZnMnO_3$ phase (Fig. 1) and the intensity of the registered signal is proportional to concentration of this phase (Fig. 8). The linewidth increases with the increase in concentration of the above phase due to stronger magnetic dipole–dipole interaction (Fig. 7). The broadening by the dipole–dipole interaction depends significantly on the concentration of the $ZnMnO_3$ phase.

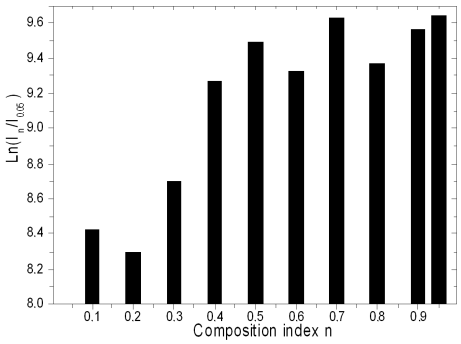

Fig. 8. Dependence of the relative integrated intensity (in logarithmic scale) on the composition index n in $n(\mathrm{MnO})/(1-n)\mathrm{ZnO}$ formula.

The EPR signal changes essentially for samples with $n > 0.5$. The g-factor parameter and linewidth shift essentially towards smaller values (Fig. 7 and Table). XRD measurements have shown that in samples with $n > 0.5$ the Mn_3O_4 and $ZnMn_2O_4$ phases are dominating. The EPR measurements have shown that the integrated intensity is lower for samples with $n = 0.6$ and $n = 0.8$ while higher values are obtained for samples $n = 0.7$ and $n = 0.95$. The linewidth increases in samples with bigger composition index n while g-factor shows an opposite tendency (Fig. 7). In sample $n = 0.80$ an additional resonance line has appeared from magnetically ordered phase that causes the dipole–dipole interaction to be stronger.

The magnetic resonance study of Mn_3O_4 and $ZnMn_2O_4$ nanoparticles was presented in Refs. [21, 22]. In Ref. [21] the structural and magnetic characteristics of the ZnMnO nanoclusters synthesized by the sol–gel method were investigated. A small quantity of $ZnMn_2O_4$ phase was also present in the studied samples. The EPR spectrum consisted of a broad line with $g \approx 1.9961$ and was attributed to Mn^{2+} ions substituting Zn^{2+}. The paramagnetic centres were assumed to exist in the interior and near the surface of the crystals. The magnetization curve measured at room temperature showed a hysteresis loop arising probably due to the presence of the $ZnMn_2O_4$ phase [21]. Nanoparticles of Mn_3O_4 produced by a novel, environmentally friendly, room-temperature route using an ionic liquid have been studied by EPR method in Ref. [22]. The production technique created a broad-size distribution of Mn_3O_4 agglomerates in the range of 8–680 nm and having various morphologies. The broad EPR line observed at room temperature did not show hyperfine splitting for Mn^{2+} and Mn^{4+} ions and had the linewidth of 2787 G and the resonance field of 4026 G. This symmetric line showed the existence of strongly interacting Mn^{2+} ions in Mn_3O_4 which was interpreted as the result of convolution of different resonance fields due to the distribution of local effective fields during dipolar interactions between particles [22].

4. Conclusions

The series of $n(\mathrm{MnO})/(1-n)\mathrm{ZnO}$ ($n = 0.05$ to 0.95) nanopowders were prepared, characterized and investigated by magnetic resonance spectroscopy. The phases ZnO and $ZnMnO_3$ dominate for $n < 0.6$ while for $n > 0.6$ the phases Mn_3O_4 and $ZnMn_2O_4$ are recorded. The EPR measurements of samples with $n < 0.6$ (except sample with $n = 0.1$) have shown that the resonance line is centered above $g_{\mathrm{eff}} = 2$ and is attributed to $ZnMnO_3$ phase. The integrated intensity increases with increasing n and for $n = 0.6$ a very strong dipole–dipole interaction is observed. A strong magnetic spin correlated system is observed for sample $n = 0.10$ and it could be associated with the formation of a low amount of $ZnMnO_3$ phase. Above $n = 0.6$ the recorded EPR line is centered below $g_{\mathrm{eff}} = 2$ and it could be attributed to $ZnMn_2O_4$ phase with the greatest content observed for samples $n = 0.7$ and $n = 0.95$. Additional resonance line is recorded for sample $n = 0.80$, probably due to the presence of small concentration of strongly correlated spins which essentially influence the broadening of the resonance line.

References

[1] T. Dietl, H. Ohno, F. Matsukura, J. Cibert, D. Ferrand, *Science* **287**, 1019 (2000).

[2] P. Sharma, A. Gupta, K.V. Rao, F.J. Owens, R. Sharma, R. Ahuja, J.M. Osorio Guillen, B. Johansson, G.A. Gehring, *Nature Mater.* **2**, 673 (2003).

[3] G. Lawes, A.S. Risbud, A.P. Ramırez, R. Seshadri, *Phys. Rev. B* **71**, 045201 (2005).

[4] S.R. Shinde, S.B. Ogale, J.S. Higgins, H. Zheng, A.J. Millis, V.N. Kulkarni, R. Ramesh, R.L. Greene, T. Venkatesan, *Phys. Rev. Lett.* **92**, 166601 (2004).

[5] M.A. Garcıa, M.L. Ruiz-Gonzalez, A. Quesada, J.L. Costa-Kramer, J.F. Fernandez, S.J. Khatib, A. Wennberg, A.C. Caballero, M.S. Martın-Gonzalez, M. Villegas, F. Briones, J.M. Gonzalez-Calbet, A. Hernando, *Phys. Rev. Lett.* **94**, 217206 (2005).

[6] K.R. Kittilstved, D.R. Gamelin, *J. Am. Chem. Soc.* **127**, 5292 (2005).

[7] K.R. Kittilstved, N.S. Norberg, D.R. Gamelin, *Phys. Rev. Lett.* **94**, 147209 (2005).

[8] D. Rubi, J. Fontcuberta, A. Calleja, L. Aragones, X.G. Capdevila, M. Segarra, *Phys. Rev. B* **75**, 155322 (2007).

[9] M. Venkatesan, C.B. Fitzgerald, J.M.D. Coey, *Nature* **430**, 630 (2004).

[10] J. Lee, J.-H. Hwang, T.T. Mashek, T.O. Mason, A.E. Miller, R.W. Siegel, *J. Mater. Res.* **10**, 2295 (1995).

[11] T. Masui, M. Yamamoto, T. Sakuta, H. Mori, G. Adachi, *J. Mater. Chem.* **10**, 353 (2000).

[12] A. Tomaszewska-Grzeda, W. Lojkowski, M. Godlewski, S. Yatsunenko, K. Drozdowicz-Tomsia, E.M. Goldys, M.R. Phillips, *Acta Phys. Pol. A* **108**, 897 (2005).

[13] S. Marczynski, N. Guskos, J. Typek, E. Grech, B. Kolodziej, *Mater. Sci. Poland* **24**, 1139 (2006).

[14] K. Kawasaki, *Prog. Theor. Phys.* **39**, 285 (1968).

[15] D.L. Huber, *Phys. Rev. B* **6**, 3180 (1972).

[16] D. Sibera, U. Narkiewicz, N. Guskos, G. Zolnierkiewicz, *J. Phys., Conf. Series* **146**, 012014 (2009).

[17] C. Liu, F. Yun, H. Morkoc, *J. Mater. Sci., Mater. Electron.* **16**, 555 (2005).

[18] Ü. Özgür, Ya.I. Alivov, C. Liu, A. Teke, M. Reshchikov, S. Dogan, V. Avrutin, S.-J. Cho, H. Morkoc, *J. Appl. Phys.* **98**, 041301 (2005).

[19] K. Sato, H. Katayama-Yoshida, *Jpn. J. Appl. Phys., Part 2* **40**, L334 (2001).

[20] U. Narkiewicz, N. Guskos, W. Arabczyk, J. Typek, T. Bodziony, W. Konicki, G. Gąsiorek, I. Kucharewicz, E. Anagnostakis, *Carbon* **42**, 1127 (2004).

[21] J.H. Li, D.Z. Shen, J.Y. Zhang, D.X. Zhao, B.S. Li, Y.M. Lu, Y.C. Liu, X.W. Fan, *J. Magn. Magn. Mater.* **302**, 118 (2006).

[22] Z. Dumas, H. Kawas, A. Baykal, M.S. Toprak, *Central Eur. J. Chem.* **7**, 555 (2009).